Suppressing the mechanical quadrature error of a quartz double-H gyroscope through laser trimming*

Zhao Ke(赵 克), Feng Li-Hui(冯立辉)†, Wang Qian-Qian(王茜蒨), Liu Ming-Zhi(刘明智), Wang Ben-Guo(王本国), Cui Fang(崔 芳), and Sun Yu-Nan(孙雨南)

School of Optoelectronics, Beijing Institute of Technology, Beijing 100081, *China*

(Received 3 June 2013; revised manuscript received 2 July 2013)

In this paper, we introduce a *z*-axis quartz gyroscope using a double-H tuning fork, which has a high sensitivity. However, it also causes a large mechanical quadrature error. The laser trimming method is used to suppress this error at quartz level. The trimming law is obtained through the finite element method (FEM). A femtosecond laser processing system is used to trim the gold balancing masses on the beams, and experimental results are basically consistent with the simulated ones. The mechanical quadrature error is suppressed by 96%, from 26.3° s^{-1} to 1.1° s^{-1}. Nonlinearity changes from 1.48% to 0.30%, angular random walk (ARW) is reduced from 2.19° $h^{-1/2}$ to 1.42° $h^{-1/2}$, and bias instability is improved by a factor of 7.7, from 197.6° h^{-1} to 25.4° h^{-1}.

Keywords: femtosecond laser trimming, micro-electro-mechanical system (MEMS) gyroscope, finite element method (FEM) simulation

PACS: 79.20.Eb, 06.30.Gv, 02.70.Dh **DOI:** 10.1088/1674-1056/22/11/117901

1. Introduction

The micro-electro-mechanical system (MEMS) gyroscope is a well-known angular rate sensor, which has been widely used in various inertia measurement fields, such as robotics, vehicle brake systems, and image stabilization.[1,2] The quartz gyroscope is a kind of MEMS gyroscope based on the piezoelectric effect, which has advantages of compact size, low cost, bulk production, and high temperature stability.[3–6] However, mechanical quadrature error, which is often larger than the angular rate signal, affects the performance of the gyroscope, such as bias stability, angular random walk (ARW), dynamic range, and temperature stability. The quadrature error is defined as the direct coupling of drive mode to sense mode.[7] The sources of quadrature error are mainly imbalances in mass, driving force, and stiffness. The imbalance in stiffness is the dominant source for the quadrature error, which is induced by inevitable micro-fabrication tolerances leading to structural defects, especially etching facets or asymmetries.

Various techniques are adopted to suppress the quadrature error in MEMS gyroscopes. One approach is to introduce a decoupled structure using specially designed proof masses and beams, but a small quadrature error still exists after decoupling.[8,9] A commonly used approach is to design an electronic feedback control circuit to inject a signal in opposite phase to the quadrature error or inject a signal to tune the stiffness matrix.[10–12] This type of compensation is limited by the stability of the device, especially in the case of devices with great imperfections. Another approach is to trim the gyroscope chip at wafer level by using a laser. This technique can suppress quadrature error efficiently when large imperfections exist in the device. It is a high-cost approach, even if it does not require any additional electronic circuitry. Laser trimming for suppressing quadrature error in a silicon MEMS gyroscope has been reported.[13] This technique has also been introduced to deal with quartz MEMS gyroscopes through some patents.[14–17] However, few papers have reported the details of laser trimming for quartz MEMS gyroscopes.

Our work focuses on the compensation of quadrature error for a quartz double-H tuning fork gyroscope at quartz level through femtosecond laser trimming, owing to its advantages, such as good controllability and high accuracy and edge quality.[18,19] This structure with four sense beams has a good ability to gather charges, leading to a high sensitivity. However, it also causes a large mechanical quadrature error. In this paper, the theory of quadrature error of the double-H gyroscope is illustrated, and the output expression is obtained in Section 2. The trimming law of the gyroscope chip is discussed through an FEM simulation in Section 3. Then, the whole trimming processes, comprising the fabrication process of micro-electroplating and the experimental setup of the femtosecond laser processing system, are introduced in Section 4. In Section 5, the experimental results of trimming through a femtosecond laser processing system are discussed, and the performances before and after laser trimming are compared and analyzed. Finally, some concluding remarks are given in Section 6.

*Project supported by the National Natural Science Foundation of China (Grant No. 61027007).

†Corresponding author. E-mail: lihui.feng@bit.edu.cn

© 2013 Chinese Physical Society and IOP Publishing Ltd

2. Theory of mechanical quadrature error of a double-H tuning fork

The structure of a double-H tuning fork gyroscope is shown in Fig. 1. It is a z-axis gyroscope. The four external beams are drive beams, and the four internal beams are sense beams. Based on the Coriolis theory, the rotation of the system on the z axis induces Coriolis acceleration along the y axis, which makes the vibrations of cross beams couple to the sense beams. Therefore, the sense beams also vibrate along the x axis. It reduces the complexity of fabricating electrodes, and four sense beams lead to a high sensitivity of the gyroscope. Gold balancing masses on drive beams are used to suppress the quadrature error, and the gold balancing masses on the sense beams are used to maintain the frequency difference between the drive mode and the sense mode.

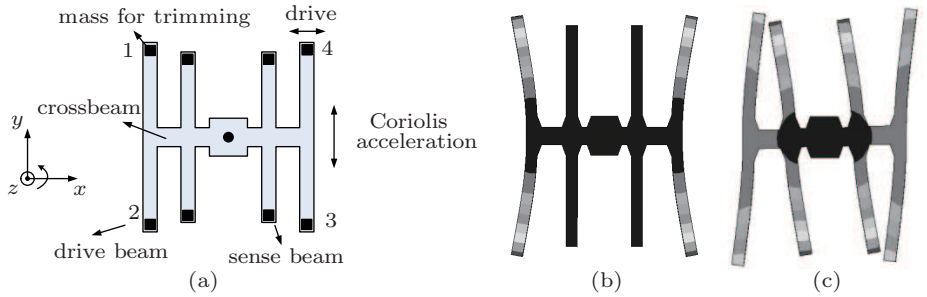


Fig. 1. Structure of a double-H gyroscope. (a) Gyroscope chip with gold masses, (b) drive mode, and (c) sense mode.

The mechanical quadrature error of the micro-quartz gyroscope is mainly induced by the imperfections in the fabrication process, which causes the gyroscope chip to be asymmetrical in some aspects, such as stiffness, damping, mass asymmetry, etc. In theory, the dynamics equation of the gyroscope is expressed as

$$\begin{bmatrix} m & 0 \\ 0 & m \end{bmatrix} \begin{bmatrix} \ddot{x} \\ \ddot{y} \end{bmatrix} + \begin{bmatrix} c_x & 0 \\ 0 & c_y \end{bmatrix} \begin{bmatrix} \dot{x} \\ \dot{y} \end{bmatrix} + \begin{bmatrix} k_x & 0 \\ 0 & k_y \end{bmatrix} \begin{bmatrix} x \\ y \end{bmatrix} = \begin{bmatrix} F_x \\ F_y \end{bmatrix}, \quad (1)$$

where m is the mass of the gyroscope chip, F_x and F_y are forces along the x axis and y axis, c_x and c_y are the dampings along the x axis and y axis, and k_x and k_y are the stiffnesses along the x axis and y axis, respectively. They are written as

$$c_x = \frac{\omega_x m}{Q_x}, \quad c_y = \frac{\omega_y m}{Q_y}, \quad k_x = \omega_x^2 m, \quad k_y = \omega_y^2 m, \quad (2)$$

where ω_x and ω_y are the resonance frequencies along the x axis and y axis, Q_x and Q_y are the quality factors along the x axis and y axis, respectively. The driving motion x is expressed as

$$x(t) = x_0 \sin(\omega_x t). \quad (3)$$

The Coriolis force F_y is expressed as

$$F_y = 2m\Omega \times \boldsymbol{v} = 2m\Omega x_0 \omega_x \cos(\omega_x t), \quad (4)$$

where Ω is the angular rate on the z axis. When there exists a fabrication error, Eq. (1) can change into

$$\begin{bmatrix} m & 0 \\ 0 & m \end{bmatrix} \begin{bmatrix} \ddot{x} \\ \ddot{y} \end{bmatrix} + \begin{bmatrix} c'_x & c_{xy} \\ c_{xy} & c'_y \end{bmatrix} \begin{bmatrix} \dot{x} \\ \dot{y} \end{bmatrix} + \begin{bmatrix} k'_x & k_{xy} \\ k_{xy} & k'_y \end{bmatrix} \begin{bmatrix} x \\ y \end{bmatrix} = \begin{bmatrix} F_x \\ F_y \end{bmatrix}, \quad (5)$$

where c_{xy} is the damping coupling coefficient and k_{xy} is the stiffness coupling coefficient. The Q factor of quartz crystal is high, so c_{xy} can be neglected.

Because of fabrication errors, the actual axes of the stiffness rotate an angle of α with respect to the original axes as shown in Fig. 2.[20] The stiffness matrix is expressed as

$$\begin{aligned} &\begin{bmatrix} k'_x & k_{xy} \\ k_{xy} & k'_y \end{bmatrix} \\ &= \begin{bmatrix} \cos\alpha & -\sin\alpha \\ \sin\alpha & \cos\alpha \end{bmatrix} \begin{bmatrix} k_x & 0 \\ 0 & k_y \end{bmatrix} \begin{bmatrix} \cos\alpha & \sin\alpha \\ -\sin\alpha & \cos\alpha \end{bmatrix} \\ &= \begin{bmatrix} k_x\cos^2\alpha + k_y\sin^2\alpha & \frac{1}{2}\sin 2\alpha(k_x - k_y) \\ \frac{1}{2}\sin 2\alpha(k_x - k_y) & k_y\cos^2\alpha + k_x\sin^2\alpha \end{bmatrix}, \end{aligned} \quad (6)$$

where $k_x = 2Ehw^3/3L^3$, $k_y = Ehw^3/4L^3$, E is the Young's modulus, h is the thickness of beam, w is the width of beam, and L is the length of beam. Equation (5) on the y axis can be simplified into

$$\ddot{y} + \frac{\omega_y}{Q_y}\dot{y} + \omega_y^2 y = 2\Omega x_0 \omega_x \cos(\omega_x t) - \frac{k_{xy} x_0}{m}\sin(\omega_x t), \quad (7)$$

whose solution is

$$y(t) = \frac{2x_0\omega_x\Omega\cos(\omega_x t - \varphi) + (k_{xy}x_0/m)\sin(\omega_x t - \varphi)}{\sqrt{(\omega_y^2 - \omega_x^2)^2 + (\omega_x\omega_y/Q_y)^2}}, \quad (8)$$

where

$$\varphi = \arctan\left(\frac{\omega_x\omega_y}{Q_y(\omega_y^2 - \omega_x^2)}\right). \quad (9)$$

According to the structure of a double-H style gyroscope, the output of the gyroscope chip is expressed by

$$U_o(t) = S\Omega\cos(\omega_x t - \phi) + \frac{\varepsilon\delta}{B}A\sin(\omega_x t - \phi),$$

where

$$\begin{aligned} S &= \frac{\varepsilon\delta}{B}8\omega_x x_0, \\ A &= 4x_0\left(\frac{k_{xy1}}{m_1} + \frac{k_{xy3}}{m_3} - \frac{k_{xy2}}{m_2} - \frac{k_{xy4}}{m_4}\right), \\ B &= \sqrt{(\omega_y^2 - \omega_x^2)^2 + \left(\frac{\omega_x\omega_y}{Q_y}\right)^2}, \end{aligned} \tag{10}$$

where ε is the piezoelectric coefficient, δ is the coupling coefficient from the crossbeam to the sense beam, S is the sensitivity, m_1, m_2, m_3, and m_4 are respectively the mass of the left upper part, left lower part, right lower part, and right upper part of the tuning fork, and k_{xy1}, k_{xy2}, k_{xy3}, and k_{xy4} are the corresponding stiffness coupling coefficients of these parts shown in Fig. 1(a). The first term on the right-hand side is the angular rate signal. The second term, which is orthogonal to the first term, is the mechanical quadrature error. Although the sensitivity is high, quadrature error is usually larger than that of the angular rate signal, which restricts the gain of amplifier. Therefore, laser trimming is used to change the mass, thereby reducing A at zero point for improving the performance.

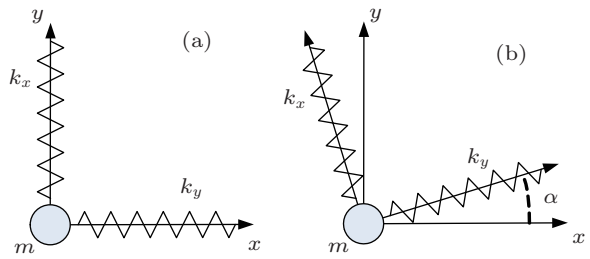


Fig. 2. Rotations of the principal axes of stiffness in (a) ideal case and (b) rotation case.

3. FEM simulation

The FEM is used to simulate the output of gyroscope chip in the case of non-angular input, and analyze the relationship between the output and removed amount of mass on the beams. It provides a basis for laser trimming.

The model of the gyroscope chip is built first. Then, the mass point is induced at the end of each fork of the model. For the reason that the highest influence on the moment of inertia I of the gyroscope is achieved, when mass is added to or removed away from the rotation axis as far as possible, according to Steiner's Theorem,[13] we have

$$I' = I + ms^2, \tag{11}$$

where s is the distance of the balancing mass from the rotation axis.

The dimensions of beams and the facets at the roots of the beams are measured by using an Olympus STM6 measuring microscope, and the mechanical quadrature error is induced by changing the size of the model according to the measurement results. Then, the balancing masses on the four drive beams are removed to obtain the output of the gyroscope and the balancing masses on the sense beams are removed to maintain the frequency difference. The balancing masses on drive beams are labeled as shown in Fig. 1. The amount of mass removed once is set to be 10% of a balancing mass. The simulation results are shown in Fig. 3.

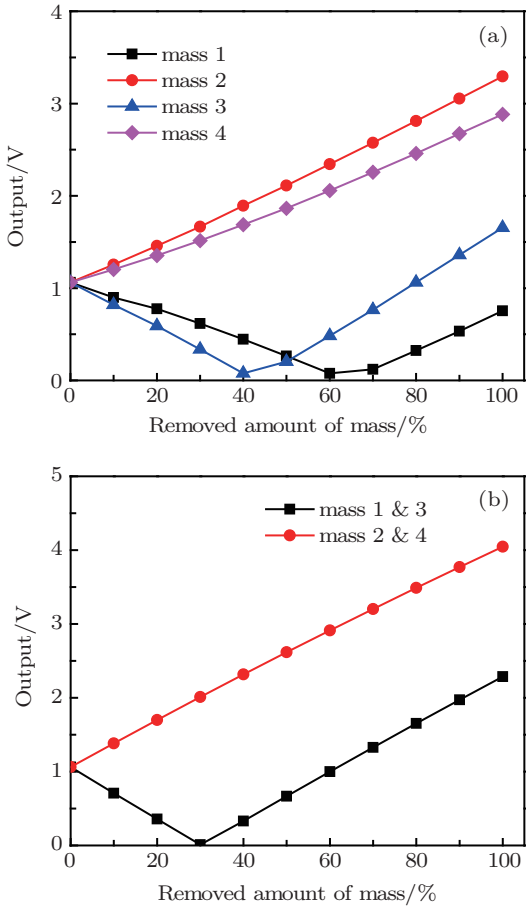


Fig. 3. (color online) Simulation results of trimming gold masses. (a) Trimming one gold mass on each beam and (b) trimming diagonal gold masses simultaneously.

The result of removing mass 1 is similar to that of mass 3. Both of them first decrease to their minimum points and then increase. On the other hand, the result of removing mass 2 is similar to that of mass 4. They all increase monotonically as the removed amount increases. Moreover, the output can be suppressed by trimming mass 1 and mass 3 simultaneously. The output decreases to 0.012 V when the removed amount is 30%. On the contrary, the output increases when removing mass 2 and 4.

In the trimming process, the removed amounts of mass 1 and mass 3 are not easy to control accurately to make the output be exactly at the minimum point. If mass 1 and mass

3 are trimmed excessively, then mass 2 and mass 4 should be trimmed. Figure 4 shows the results of trimming mass 2 and mass 4, when the removed amounts of mass 1 and mass 3 are 40%, 60%, and 80%, respectively.

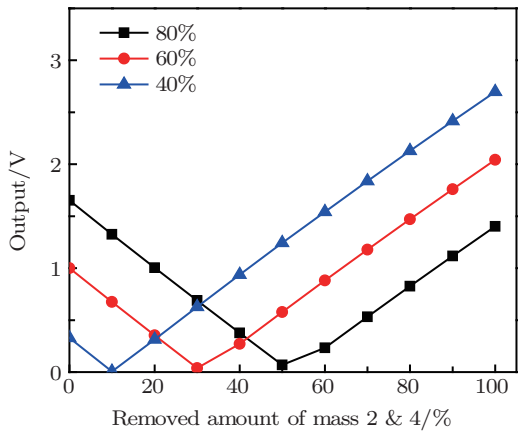


Fig. 4. (color online) Simulation results of trimming mass 2 and 4, when trimming mass 1 and 3 excessively.

Moreover, the simulation results by inducing different mechanical quadrature errors are similar. In conclusion, the laws of the output through removing balancing masses on diagonal beams are similar. A pair of them increases monotonically, and the other pair first decreases to the minimum point and then increases. The output can be suppressed to the minimum point through trimming the latter pair properly. If the latter pair of balancing masses is trimmed excessively, then the former pair of balancing masses should be trimmed.

4. Experimental setup

The whole experiment consists of the following procedures: tuning fork making, electroplating gold balancing masses, femtosecond laser trimming, and measurement of the output signal in the detecting circuit.

In the fabrication process, Cr/Au films were deposited on the quartz wafer. The adhesion of Au films was improved by depositing them on Cr layers, so that the effect of the stress difference between different materials can be weakened and the long-term performance of the gyroscope can be guaranteed. The gold balancing mass was electroplated on Cr/Au films at the end of each beam, and the size is 300 μm×180 μm×8 μm. The photoresist AZ4620 was used to make the mask for electroplating through exposure by an ABM mask aligner system. Sulfite is the main ingredient of electroplating solution, owing to its low pollution and proper surface quality of electroplated layer.

A femtosecond laser processing system made by the Newport Corporation was used to trim the gold balancing masses on the beams. The system is shown in Fig. 5. The femtosecond laser system contains a Tsunami laser oscillator and a Spitfire Pro laser amplifier. A computer control system was used to set parameters such as wavelength, output power, and motion of platform. The wavelength is set to be 586 nm, the pulse energy is 3 μJ, the pulse duration is 50 fs, and the repetition frequency is 1 kHz. The speed of the platform was set to be 300 μm/s. The displacements along the x axis and y axis are 200 μm and 20 μm, respectively. The ablation depth was controlled below 7 μm. The gyroscope was located on the platform, the supply voltage is ±9.0 V, and the output signal was observed by using a Tektronix oscilloscope. The measurement value of the mechanical quadrature error is the output of the amplifier as shown in Fig. 6.

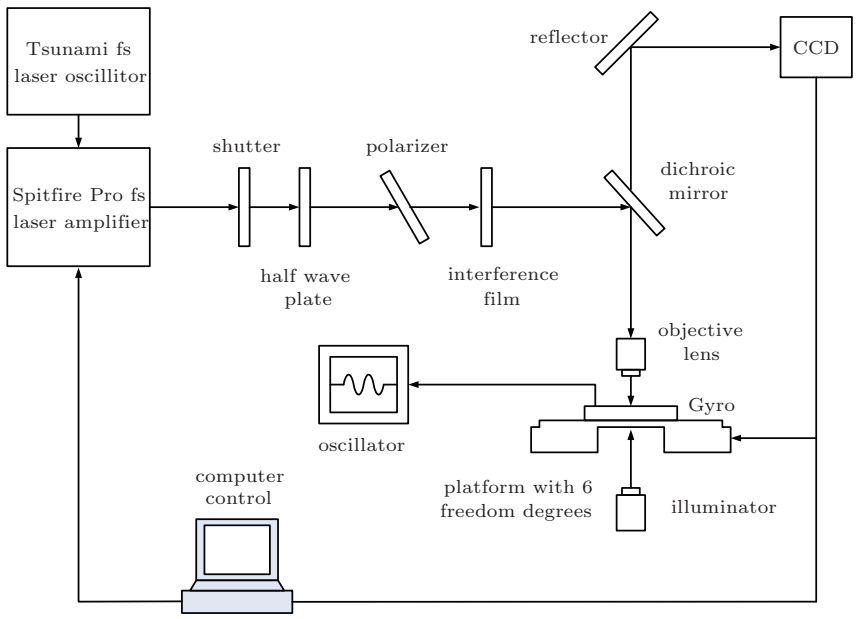


Fig. 5. Schematic diagram of the laser processing system.

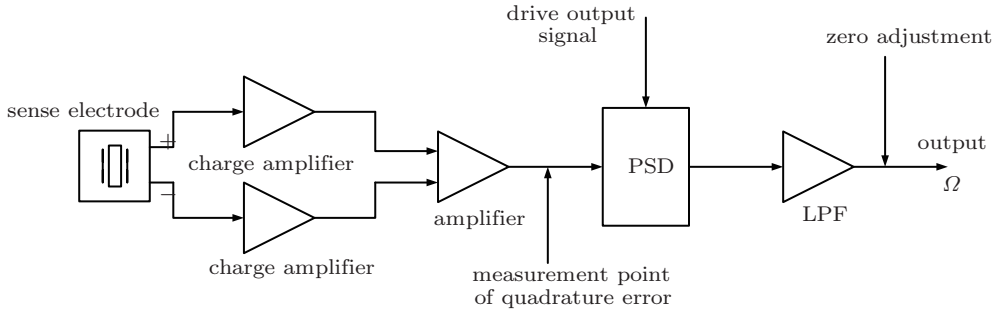


Fig. 6. Detection circuit of the double-H gyroscope.

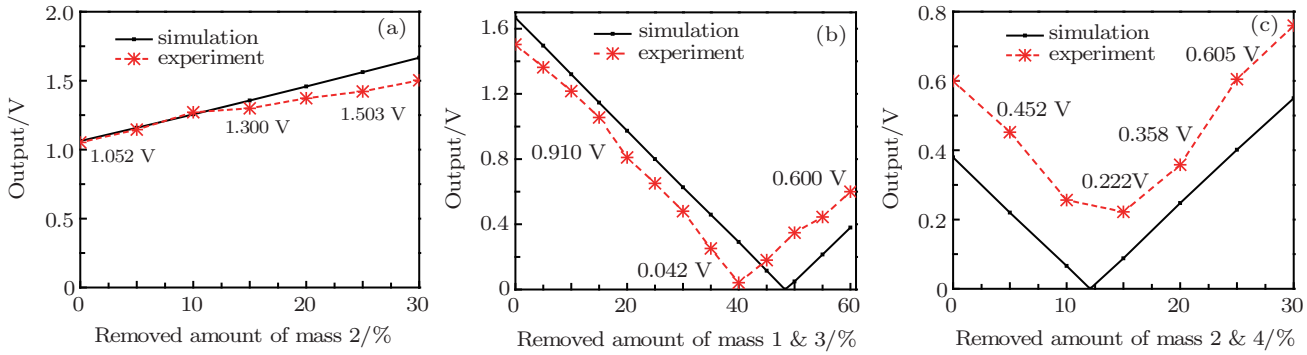


Fig. 7. (color online) Experimental results of (a) trimming mass 2, (b) trimming mass1 and 3, and (c) trimming mass 2 and 4 when mass is trimmed excessively.

Finally, the gyroscope is located on the rotation platform in the thermostat, and the outputs in a range of $\pm 200^\circ$ s^{-1} are measured at the sample rate of 2 Hz with a PCI-6280 data acquisition device made by National Instrument. Then, zero-rate output is measured, which takes 4 h at the sample rate of 200 Hz.

5. Results and discussion

Through laser trimming, the mechanical quadrature error is suppressed efficiently by 96% from 1.052 V to 0.042 V, and the corresponding zero bias output is 26.3° s^{-1} and 1.1° s^{-1}, respectively. The experimental results are shown in Fig. 7, which are mainly correlated with the simulation results. The amount of mass removed through laser trimming is about 5% (ablation size $200\times20\times5.5$ μm^3) of a gold balancing mass ($300\times180\times8$ μm^3) in each step. In Fig. 7(c), the minimum point of the quadrature error is a little higher than the simulation result, partly due to the errors of the model in the simulation, and partly due to the in-phase errors in the output of gyroscope. The capacitive coupling error is the main source of the in-phase errors. The waveforms of the preamplifier outputs before and after trimming are shown in Fig. 8. The quadrature error is a sinusoidal wave signal. When it is suppressed to a small value, the square-wave signal in the output emerges with the same wave form as that of the driving signal. It is the in-phase error, especially capacitive coupling error. Another cause for in-phase errors is the damping error, which induces c_{xy} in Eq. (5), when the gyroscope works in an open-air environment. It can be neglected because of the high Q factor of the quartz resonator. Figure 9 shows the relations between these signals. U stands for the output, U_a is the angular rate signal and $U_a = 0$ in the trimming process, U_{in} is the in-phase error, U_q is the quadrature error, and

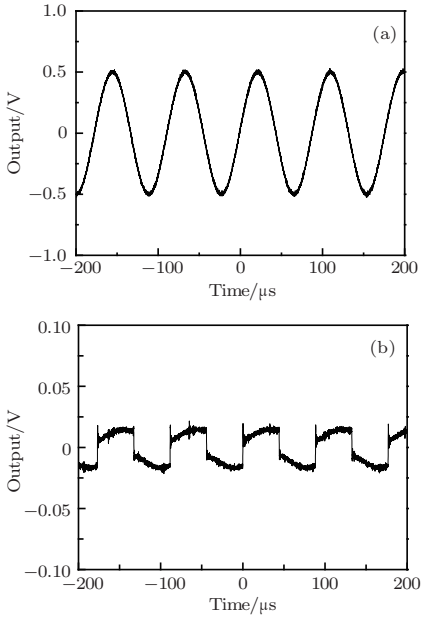


Fig. 8. Outputs of the preamplifier (a) before and (b) after laser trimming.

$|U| = [U_q^2 + (U_{in} + U_a)^2]^{1/2}$. When U_q decreases, U_{in} is the main source of the errors, so the amplitude of output U is not reduced to the lowest point as shown by the simulation results.

Allan variance graphs before and after trimming are shown in Fig. 10. The performances are presented in Table 1. Frequency difference and scale factor change a little, because the quantity of mass changes is too small to have crucial effect on the motions of drive beams and sense beams. The scale factor is also influenced by the gain of the amplifier, when the quadrature error is so large that the amplifier becomes saturated. Nonlinearity, ARW, and bias instability are influenced significantly by the quadrature error. They are improved by 1.18%, 1.5 times, and 7.7 times, respectively. This is a result of reducing influences on sense beams by quadrature errors. Larger phase error is induced in the phase-sensitive demodulator which affects the linearity of the output, when the quadrature error is higher. Meanwhile, more extra noises are also injected to the detect circuit, affecting the ARW. In addition, the drift of the quadrature error causes the zero output to be instable, leading to a high bias instability. Therefore, the performance is improved as the quadrature error is suppressed. However, the ARW and bias instability are still high, which can be suppressed further through digital circuits.

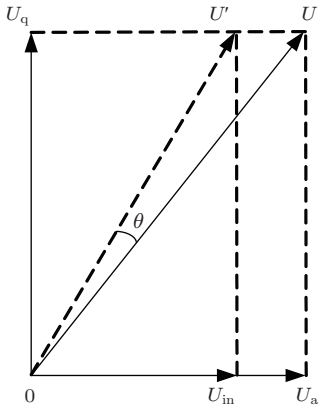


Fig. 9. Relationship between the angular rate signal and errors.

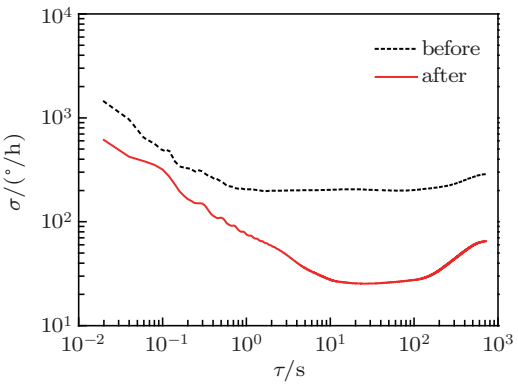


Fig. 10. (color online) Allan variance graphs before and after laser trimming.

Table 1. Performance parameters before and after trimming.

Performance parameters	Before trimming	After trimming
Scale factor/mV/(°/s)	17.5	19.8
Frequency difference/Hz	162	165
Nonlinearity/%	1.48	0.30
Bias instability/(°/h)	197.6	25.4
ARW/(°/$\sqrt{\mathrm{h}}$)	2.19	1.42

6. Conclusions

In this paper, we present the compensation of the mechanical quadrature error for a quartz double-H tuning fork gyroscope at the quartz level. This structure has high sensitivity, leading to high quadrature error. The theory of the double-H gyroscope is analyzed and the finite element method is used to simulate the mass trimming process. A femtosecond laser processing system is used to trim the quartz tuning fork, and the mechanical quadrature error is reduced by 96%, from 26.3° s^{-1} to 1.1° s^{-1}. The experimental results are basically consistent with the simulation ones. The performance is improved after the quadrature error is suppressed through laser trimming. Nonlinearity changes from 1.48% to 0.30%, ARW is reduced from 2.19° $h^{-1/2}$ to 1.42° $h^{-1/2}$, and the bias instability is improved by a factor of 7.7.

There still exist in-phase errors, especially capacitive coupling errors, which should be identified and eliminated. In addition, the laser processing system can be improved to be more efficient and accurate to suppress the quadrature error. The circuit will be digitalized to reduce the ARW and bias instability further in our future work.

Acknowledgment

The authors acknowledge Professor Lan Jiang in School of Mechanical Engineering in Beijing Institute of Technology for his assistance.

References

[1] Nonomura Y, Fujiyoshi M, Omura Y, Fujitsuka N, Mizuno K and Tsukada K 2006 *Sensor. Actuat. A* **132** 42
[2] Hu Z X, Gallacher B J, Burdess J S, Fell C P and Townsend K 2011 *Sensor. Actuat. A* **167** 249
[3] Madni A M, Costlow L E and Knowles S J 2003 *IEEE Sens. J.* **3** 569
[4] Xie L Q, Wu X Z and Li S Y 2010 *Sensors* **10** 1573
[5] Parent A, Traon O L, Masson S and Foulgoc B L 2007 *IEEE Sensors Conference*, October 28–31, 2007 Atlanta, Georgia, USA, p. 876
[6] Wu X Z, Xie L Q, Xing J C, Dong P T, Wang H X and Su J B 2012 *IEEE Sen. J.* **12** 1246
[7] Tatar E, Alper S E and Akin T 2012 *J. Microelectromech. Syst.* **21** 656
[8] Alper S E, Temiz Y and Akin T 2008 *J. Microelectromech. Syst.* **17** 1418
[9] Geiger W, Butt W U, Gaisser A, Frech J, Braxmaier M, Link T, Kohne A, Nommensen P, Sandmaier H and Lang W 2002 *Sensor. Actuat. A* **95** 239
[10] Descharles M, Guerard J, Kokabi H and Le Traon O 2012 *Sensor. Actuat. A* **181** 25
[11] Saukoski M, Aaltonen L and Halonen K A I 2007 *IEEE Sens. J.* **7** 1639
[12] Painter C C and Shkel A M 2003 *IEEE Sens. J.* **3** 595

[13] Günthner S, Egretzberger M, Kugi A and Kapser K 2006 *IEEE Sens. J.* **6** 596

[14] Knowles S J and Moore R H 2010 European Patent 1174681B1 [2010-6-2]

[15] Tchertkov I L, Aston S E H, August R J and Jaffe R 2009 U.S. Patent 7548318B2 [2009-6-16]

[16] Knowles S J and Moore R H 2009 U.S. Patent 7523537B1 [2009-4-28]

[17] Kawauchi O, Miyazawa S, Takayama K and Yamaguchi K 2007 U.S. Patent 7207221B2 [2007-4-24]

[18] Li C, Argument M and Tsui Y Y 2000 *Applications of Photonic Technology*, December 15, 2000 Quebec City, Canada, p. 1194

[19] Momma C, Chichkov B N and Nolte S 1996 *Opt. Commun.* **129** 134

[20] Painter C C and Shkel A M 2002 *Smart Structures and Materials* 2002*: Smart Electronics, MEMS, and Nanotechnology*, March 18–20, 2002 San Diego, CA, USA, p. 157